Antiviral Research 212 (2023) 105571

Contents lists available at ScienceDirect

Antiviral Research

journal homepage: www.elsevier.com/locate/antiviral

Design and characterization of novel SARS-CoV-2 fusion inhibitors with N-terminally extended HR2 peptides

Yue Hu [a,1], Yuanmei Zhu [a,1], Yanying Yu [b,1], Nian Liu [a], Xiaohui Ju [b], Qiang Ding [b,**], Yuxian He [a,*]

[a] NHC Key Laboratory of Systems Biology of Pathogens, Institute of Pathogen Biology and Center for AIDS Research, Chinese Academy of Medical Sciences and Peking Union Medical College, Beijing, 100730, China
[b] Center for Infectious Disease Research, School of Medicine, Tsinghua University, Beijing, 100084, China

ARTICLE INFO

Keywords:
SARS-CoV-2
Fusion inhibitors
Peptides
Lipopeptides

ABSTRACT

Development of potent and broad-spectrum antivirals against SARS-CoV-2 remains one of top priorities, especially in the case of that current vaccines cannot effectively prevent viral transmission. We previously generated a group of fusion-inhibitory lipopeptides, with one formulation being evaluated under clinical trials. In this study, we dedicated to characterize the extended N-terminal motif (residues 1161–1168) of the so-called spike (S) heptad repeat 2 (HR2) region. Alanine scanning analysis of this motif verified its critical roles in S protein-mediated cell-cell fusion. Using a panel of HR2 peptides with the N-terminal extensions, we identified a peptide termed P40, which contained four extended N-terminal residues (VDLG) and exhibited improved binding and antiviral activities, whereas the peptides with further extensions had no such effects. Then, we developed a new lipopeptide P40-LP by modifying P40 with cholesterol, which exhibited dramatically increased activities in inhibiting SARS-CoV-2 variants including divergent Omicron sublineages. Moreover, P40-LP displayed a synergistic effect with IPB24 lipopeptide that was designed containing the C-terminally extended residues, and it could effectively inhibit other human coronaviruses, including SARS-CoV, MERS-CoV, HCoV-229E, and HCoV-NL63. Taken together, our results have provided valuable insights for understanding the structure-function relationship of SARS-CoV-2 fusion protein and offered novel antiviral strategies to fight against the COVID-19 pandemic.

1. Introduction

The global pandemic of COVID-19 has lasted over three years and caused more than six million death cases (https://covid19.who.int/). The pathogen SARS-CoV-2 continues to spread with evolutionary mutations, resulting in many viral variants that challenge the efficacies of vaccines and neutralizing antibody therapies (Cao et al., 2022; Markov et al., 2022; Qu et al., 2022; Shrestha et al., 2022; Uraki et al., 2022; Wang et al., 2021). After Alpha (B.1.1.7), Beta (B.1.351), Gamma (P1), and Delta (B.1.617.2), Omicron (B.1.1.529) emerged as the fifth variant of concern (VOC), exhibiting the largest mutations, higher transmissibility and more prone to immune evasion (Fan et al., 2022; Guo et al., 2022). Currently, Omicron has already evolved into distinct sublineages, with BA.2- and BA.5-based variants predominant worldwide, calling for urgent development of effective broad-spectrum antiviral approaches.

Viral fusion protein-derived peptides are potent entry inhibitors by blocking assembly of a six-helical bundle (6-HB) structure between two heptad repeat regions (HR1 and HR2) of the protein, as exemplified by anti-HIV drug enfuvirtide (T-20), a 36-mer native HR2 peptide of envelope (Env) glycoprotein gp41 (Lalezari et al., 2003; Wild et al., 1994). This strategy has been widely applied to develop novel inhibitors against HIV and many other enveloped viruses, including emerging human coronaviruses (CoVs) (Tang et al., 2020). In the past decade, we have devoted to develop HIV fusion inhibitors, with Sifuvirtide and Lipovirtide under clinical trials (Chong et al., 2019; He et al., 2008a, 2008b; Xue et al., 2022). After SARS-CoV-2 outbreak, we immediately initiated projects to develop antivirals, generating a group of fusion-inhibitory

* Corresponding author.
** Corresponding author.
E-mail addresses: qding@tsinghua.edu.cn (Q. Ding), yhe@ipb.pumc.edu.cn (Y. He).
[1] These authors contributed equally to this work.

https://doi.org/10.1016/j.antiviral.2023.105571
Received 19 January 2023; Received in revised form 18 February 2023; Accepted 23 February 2023
Available online 1 March 2023
0166-3542/© 2023 The Authors. Published by Elsevier B.V. This is an open access article under the CC BY license (http://creativecommons.org/licenses/by/4.0/).

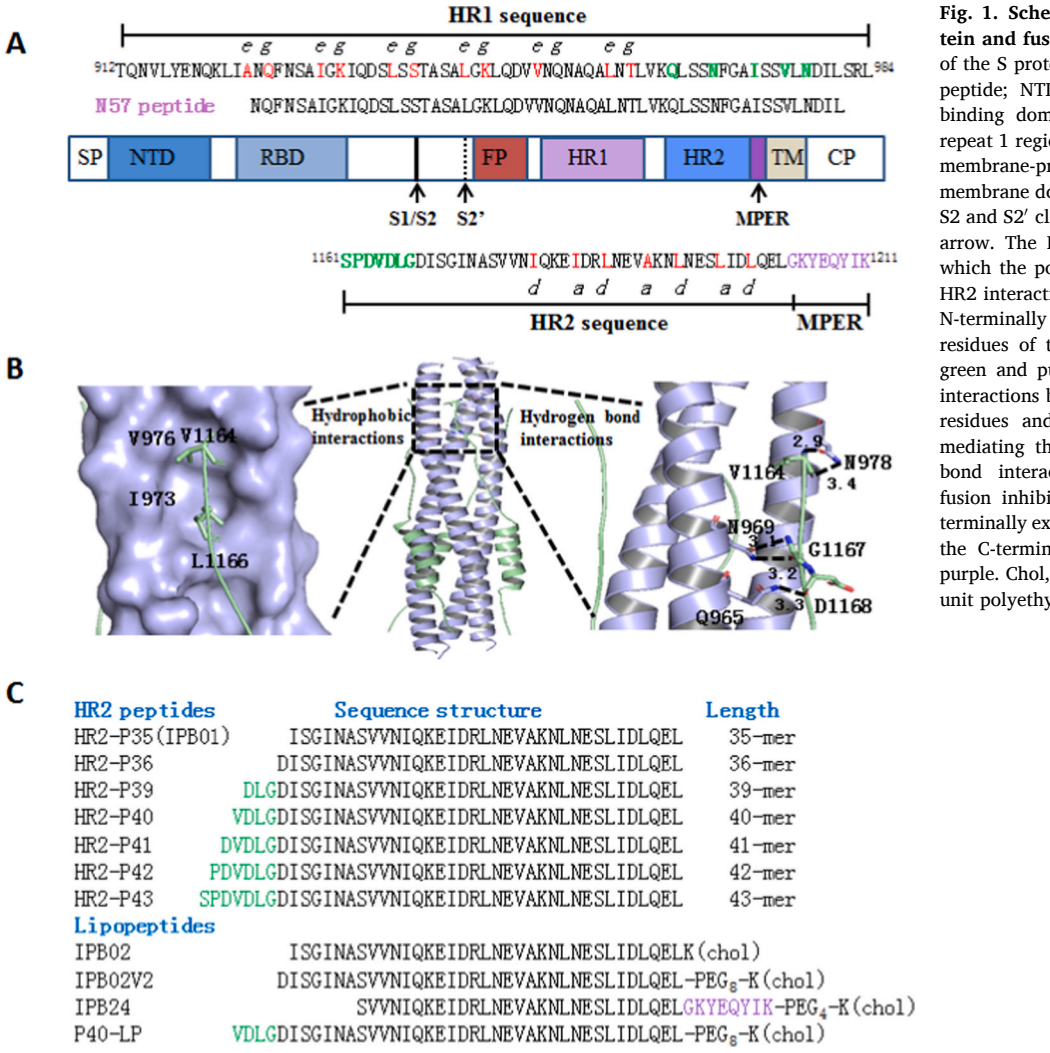

Fig. 1. Schematic diagram of SARS-CoV-2 S protein and fusion inhibitors. (**A**) Functional domains of the S protein and HR1/HR2 sequences. SP, signal peptide; NTD, N-terminal domain; RBD, receptor-binding domain; FP, fusion peptide; HR1, heptad repeat 1 region; HR2, heptad repeat 2 region; MPER, membrane-proximal external region; TM, transmembrane domain; CP, cytoplasmic peptide. The S1/S2 and S2′ cleavage sites and MPER are marked with arrow. The HR1 and HR2 sequences are listed, in which the potential residues that mediate the HR1-HR2 interactions in 6-HB are colored in red, and the N-terminally extended residues and C-terminal MPER residues of the HR2 core sequence are colored in green and purple, respectively. (**B**) Analysis of the interactions between the N-terminally extended HR2 residues and HR1 target, in which the residues mediating the specific hydrophobic and hydrogen-bond interactions are marked. (**C**) HR2-derived fusion inhibitor peptides and lipopeptides. The N-terminally extended residues are marked in green and the C-terminally extended residues are colored in purple. Chol, cholesterol; PEG8 or PEG4, 8-unit or 4-unit polyethylene glycol.

peptides and lipopeptides with very potent and broad-spectrum activities (Yu et al., 2021a, 2021b; Zhu et al., 2020, 2021, 2022a, 2022b). As illustrated in Fig. 1, IPB01 and IPB02 based inhibitors were designed with the HR2 core sequence of S2 fusion protein, whereas IPB24 contained a membrane proximal external region (MPER). In an advanced stage, a lipopeptide-based formulation is currently under clinical trials in China, which evaluate both its therapeutic and preventive efficacies administrated through nebulization (ChiCTR2300068170).

Recent studies have demonstrated that HR1 and HR2 derived peptides of SARS-CoV-2 fusion protein (S2 subunit) adopts a typical post-fusion 6-HB structure, in which the HR1 α-helices forms an interior core with grooves that are antiparallelly packed by the HR2 α-helices (Sun et al., 2020; Xia et al., 2020a; Yang et al., 2022b). Notably, the N-terminal motif of HR2 forms a well-defined conformation, in which several residues (V1164, L1166, G1167 and D1168) make extensive hydrophobic or hydrogen-bond interactions with the C-terminal site of HR1 groove, implying its roles in viral infectivity and HR2-based antivirals. Very recently, Yang and colleagues reported that an N-terminally extended HR2 peptide, namely P42 in Fig. 1C, exhibited a nanomolar (nM) inhibitory activity and was ~100-fold more potent than the previously characterized HR2 core peptide P36 (Yang et al., 2022a), which obviously differed from our results. In order to clarify the contradiction and systemically exploit the mechanisms of SARS-CoV-2 fusion and its inhibition, we focused on characterizing the function of HR2 N-terminal motif in cell fusion and viral entry. The results demonstrated the importance of the N-terminal residues on S protein-driven cell fusion and designing of fusion-inhibitory peptides. A novel lipopeptide, termed P40-LP, was accordingly designed with potent and broad-spectrum activity against SARS-CoV-2 and other human coronaviruses (SARS-CoV, MERS-CoV, HCoV-229E, and HCoV-NL63). Remarkably, P40-LP had different levels of synergistic effects with the C-terminally extended inhibitor IPB24, thus providing a new strategy to fight against the COVID-19 pandemic.

2. Materials and methods

2.1. Plasmids and cells

Plasmids encoding the wild-type (WT) and mutant S proteins of SARS-CoV-2 were a kind gift from Linqi Zhang at the Tsinghua University (Beijing, China). Plasmids encoding the S proteins with a single, double or triple mutations and 293T/ACE2 cells were constructed in our laboratory and used in the previous studies (Yu et al., 2021a; Zhu et al., 2022a). HEK293T, Huh-7 cells, and Caco-2 cells were purchased from the American type culture collection (ATCC) (Rockville, MD, USA). Cells were cultured in complete growth medium consisting of Dulbecco's minimal essential medium (DMEM) supplemented with 10% fetal bovine serum (FBS), 100 U/ml of penicillin/streptomycin, 2 mM L-glutamine, and 1 mM sodium pyruvate under 5% CO_2 and 37 °C.

2.2. Peptides and lipopeptides

A panel of HR2 peptides (P35~P43) and HR1 peptide N57 (Fig. 1C) were synthesized on rink amide 4-methylbenzhydrylamine (MBHA) resin using a standard solid-phase 9-flurorenylmethoxycarbonyl (FMOC) protocol as described previously (Yu et al., 2021a). Lipopeptides (P40-LP, IPB02V2, IPB24) were prepared by amidation of a C-terminal lysine side chain with cholesteryl succinate monoester (Yu et al., 2021a), in which 8-unit polyethylene glycol (PEG_8) was introduced as a flexible linker. All the peptides were acetylated at the N-terminus prior to resin cleavage, followed by purification with reverse-phase high-performance liquid chromatography (RP-HPLC) to homogeneity of greater than 95%. The molecular weight (MW) of peptides was characterized by mass spectrometry (MS) for correction.

2.3. Alanine scanning analysis

The functionalities of the HR2 residues 1161–1168 were analyzed by site-directed mutagenesis as described previously (Yu et al., 2021a). The forward and reverse primers with 16–28 nucleotides were designed with specific mutations and occupied the same starting and ending positions on the opposite strands of a codon-optimized S gene template cloned in a pcDNA3.1 vector. PCR amplification was conducted in a 25-μl reaction volume using 100 ng of denatured plasmid template, 50 pM upper and lower primers, and 5 U of high-fidelity polymerase PrimeStar (TaKaRa, Dalian, China), including one cycle of denaturation at 98 °C for 5 min, 25 cycles of 98 °C for 10 s, 68 °C for 9 min, and a final extension at 72 °C for 10 min. The amplicons were then treated with restriction enzyme DpnI for 3 h at 37 °C, and DpnI-resistant molecules were recovered by transforming Trans 2-Blue Chemically Competent Cells to antibiotic resistance (TransGen Biotech, Beijing, China). The desired mutations were confirmed by DNA sequencing.

2.4. Western blotting assay

The expression profiles of the S proteins with HR2 mutations in transfected cells or PsV particles were examined by western blotting as described previously (Zhu et al., 2022b). In brief, 5×10^5/ml 293T cells were seeded in a 6-well plate and transfected by an S-expressing plasmid. After 48 h, transfected cells were collected and lysed for 30 min on ice, then centrifuged with 12,000×*g* at 4 °C for 1h to remove insoluble materials. The lysates were diluted and adjusted to a same protein concentration by BCA Protein Assay Kit (Thermo Scientific, Rockford, IL, USA). Proteins in lysates were separated by SDS-PAGE and transferred to a nitrocellulose membrane. After blocking with 5% nonfat dry milk solution in Tris-buffered saline (TBS, pH 7.4) at room temperature for 1 h, the membrane was washed and then incubated with a rabbit anti-S1 or S2 polyclonal antibody (SinoBiological, Beijing, China) overnight at 4 °C. After washes, the membrane was incubated with IRDye 680LT or IRDye 800CW goat-anti-rabbit IgG at room temperature for 2 h. β-actin was detected as an internal control with a mouse anti--β-actin monoclonal antibody (Sigma, St. Louis, MO, USA) and IRDye 680LT donkey-anti-mouse IgG. The membrane was then scanned using the Odyssey infrared imaging system (LI-COR Biosciences, Lincoln, NE, USA).

In order to analyze the incorporation of S protein, the cell culture supernatants containing PsV particles were concentrated by 30KD ultrafiltration centrifuge tube and then precipitated with 3% PEG-6000 overnight at 4 °C. After centrifuging at 14,000×*g* at 4 °C for 1h, the viral particles were lysed overnight at 4 °C and centrifuged at 20, 000×*g* at 4 °C for 1h to remove insoluble materials. The same amounts of viral lysates were normalized by P24 antigen and then subjected to SDS-PAGE and immunoblotting as described above. P24 was detected with a rabbit anti-P24 polyclonal antibody (SinoBiological, Beijing, China) and IRDye 680LT donkey-anti-rabbit IgG.

2.5. Circular dichroism spectroscopy

The α-helicity and thermostability of a peptide or lipopeptide as well as their complexes with HR1-derived target mimic peptide N57 were detected by circular dichroism (CD) spectroscopy as described previously (Zhu et al., 2020). Briefly, peptides were diluted with a final concentration of 10 μM in phosphate-buffered saline (PBS, pH 7.2) and incubated at 37 °C for 30min. CD spectrum was obtained on Jasco spectropolarimeter model J-815 using a 1-nm bandwidth with a 1 nm step resolution from 195 to 270 nm at 20 °C. The spectra were corrected by subtracting a solvent blank, and the α-helical content was calculated from the CD signal by dividing the mean residue ellipticity [θ] at 222 nm by with a value of −33,000 deg cm2 $dmol^{-1}$ that corresponds to a 100% helix. The ellipticity change was monitored during thermal denaturation at 222 nm from 20 to 98 °C at a rate of 2 °C/min, and melting temperature (T_m) was defined as the midpoint of thermal unfolding transition.

2.6. Native-polyacrylamide gel electrophoresis

HR2 peptides and their interactions with HR1-derived peptide N57 were visualized by native polyacrylamide gel electrophoresis (N-PAGE) as described previously (Zhu et al., 2020). Briefly, an HR2 peptide at 40 μM was mixed with N57 at 80 μM and incubated at 37 °C for 30 min. The mixture was added with Tris-glycine native loading buffer at a ratio of 1:1 and loaded onto a 15 x 1.5-mm 20% Tris-glycine gel at 25 μl per well. Gel electrophoresis was conducted under a 120-V constant voltage at 4 °C for 4 h. Then, the gel was stained by Instant Blue Coomassie Protein Stain (Abcam, Cambridge, UK) and imaged with a Bio-Rad imaging system (Bio-Rad, Hercules, CA, USA). The intensity of peptide band was analyzed by image J. The binding rate of an HR2 peptide with N57 was obtained by 100% minus the percentage of remaining unbound peptide.

2.7. Cell-cell fusion assay

S protein-mediated cell-cell fusion activity was first determined by a green fluorescent protein (GFP)-based cell-cell fusion assay. Briefly, 293T cells (effector cells) were cotransfected with an S-expressing plasmid and a GFP-expressing plasmid, then incubated for 48 h at 37 °C, whereas 293T cells transfected with GFP plasmid only were used as control. 5×10^4 of 293T/ACE2 and Huh-7 cells (target cells) were placed in 96-well plates and cultured overnight at 37 °C. On the next day, 1×10^4 effector cells were added to target cells for co-incubation for 5 h at 37 °C. Under an inverted fluorescence microscope, three fields were randomly selected in each well to count the number of fused and unfused cells and take pictures to calculate the fusion rate.

The S-mediated cell-cell fusion was also measured by a dual-split-protein (DSP)-based cell-cell fusion assay (Zhu et al., 2022b). 1.5×10^4 293T cells were seeded in a 96-well plate as effector cells, 1.5×10^5/ml of 293T/ACE2, Huh-7 or Vero E6 cells were cultured in a 10-cm culture dish as target cells. After culturing at 37 °C overnight, effector cells were cotransfected with the S-expressing plasmid and a $DSP_{1\text{-}7}$ plasmid, target cells were transfected with a $DSP_{8\text{-}11}$ plasmid, and then incubated for 24 h at 37 °C. To determine the inhibitory activity of peptides or lipopeptides, a serially 3-fold diluted inhibitor was added to the effector cells and incubated for 1 h, whereas the target cells were resuspended (3×10^5/ml) in prewarmed culture medium containing 20 ng/ml EnduRen live cell substrate (Promega, Madison, WI, USA) and incubated for 30 min. Then, a total of 3×10^4 target cells were transferred to the effector cells, and the cell mixtures were spun down to facilitate cell-cell contact. Luciferase activity was measured using luciferase assay reagents and a luminescence counter (Promega).

2.8. Single-cycle infection assay

Infectivity of various SARS-CoV-2 pseudoviruses (PsV) in 293T/

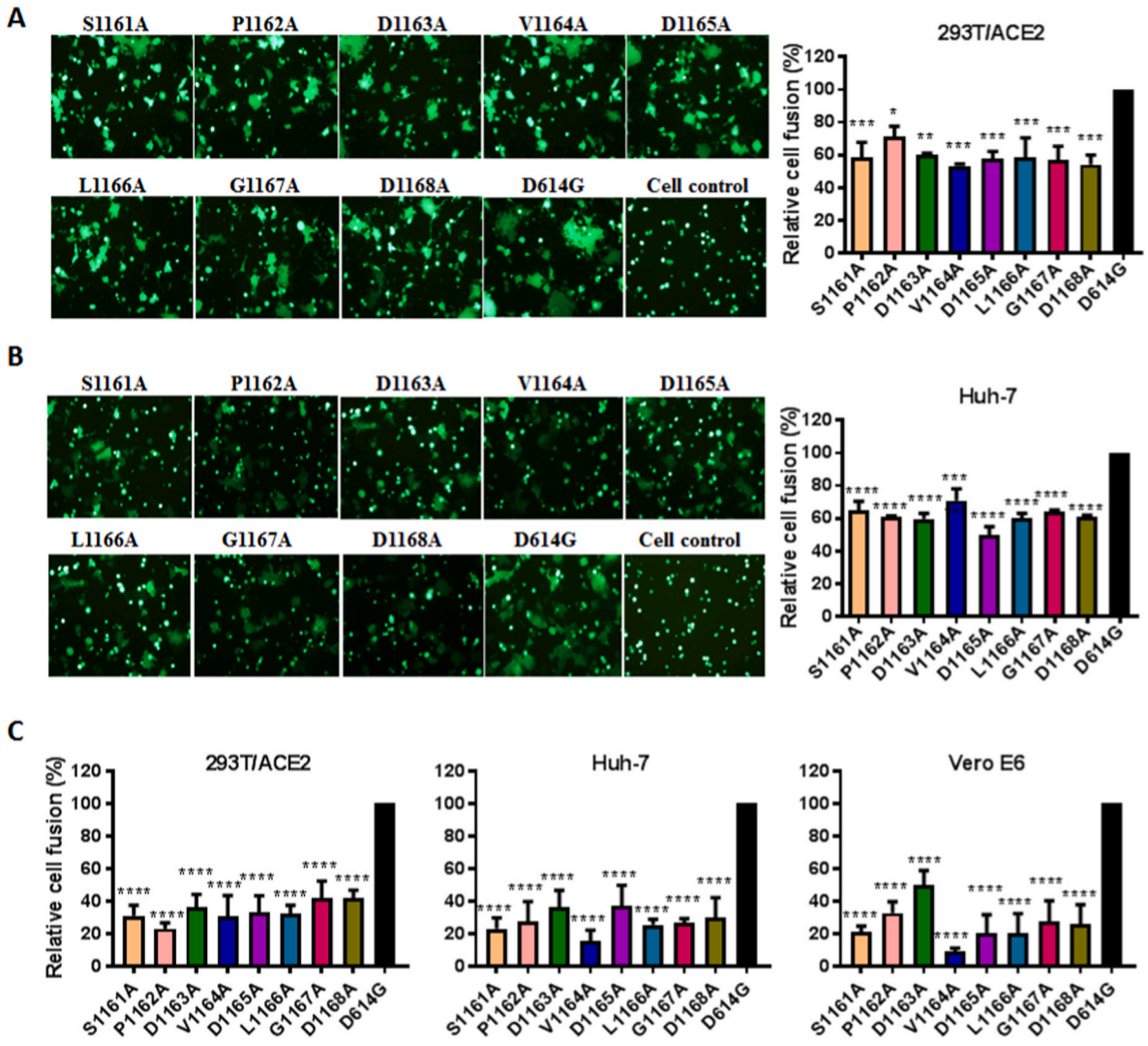

Fig. 2. Fusogenic activities of the S mutants with HR2 mutations. The fusogenicity of various S mutants was determined on 293T/ACE2 cells (**A**) or Huh-7 cells (**B**) by a GFP-based cell-cell fusion assay. (**C**) The fusogenicity of the S mutants on 293T/ACE2, Huh-7, or Vero E6 cells was determined by a DSP-based cell fusion assay. In comparison, the fusogenicity of the S protein with a single D614G mutation (D614G reference) was treated as 100% and the relative fusion rate of a mutant was accordingly calculated, and statistical comparisons were conducted by one-way ANOVA with Dunnett's multiple comparisons test.

ACE2 or Huh-7 as target cells was determined by a single-cycle infection assay as described previously (Zhu et al., 2022b). To package a PsV, 5×10^6 293T cells grown in 15 ml of growth medium in a T-75 culture flask were cotransfected with the S-expressing plasmids and a lentiviral backbone plasmid (pNL4-3. luc.RE) that encodes an Env-defective, luciferase reporter-expressing HIV-1 genome. After culturing 48 h, cell supernatants with released PsV particles were collected, filtrated and stored at −80 °C. The 50% tissue culture infectious dose ($TCID_{50}$) of PsV was determined in target cells. To compare the infectivity, PsV particles were normalized to a fixed amount of p24 antigen and their relative infection was calculated. To measure the inhibitory activity of peptides or lipopeptides, a serially 3-fold diluted inhibitor was mixed with an equal volume of PsV at 500 $TCID_{50}$ and incubated at 37 °C for 30 min; then, the inhibitor-virus mixture was added to 293T/ACE2 or Huh-7 cells (1×10^4 cells/well). After incubation at 37 °C for 48 h, the target cells were collected and lysed in reporter lysis buffer (Promega), and the luciferase activity was measured as described above.

2.9. SARS-CoV-2 trVLP production and infection

To evaluate the inhibitory activity of peptides or lipopeptides against SARS-CoV-2 infection, the SARS-CoV-2 transcription- and replication-component virus-like-particles (trVLPs) system, which recapitulate the complete viral life cycle by genetic transcomplementation was applied as described previously (Ju et al., 2021). Briefly, the nucleocapsid (N) gene of trVLP was replaced by a GFP reporter gene, which then trans-complement to the packaging cell line Caco-2 for ectopic expression of N. The complete viral life cycle of trVLP can be recapitulated and confined to Caco-2-N cells, with GFP signal serving as surrogate readout for viral infection. The cDNA of D614G mutant or Omicron trVLP was ligated *in vitro* as the template to synthesize the genomic RNA by *in vitro* transcription using mMESSAGE mMACHINE T7 Transcription Kit (ThermoFisher Scientific) and then electroporated into Caco-2-N cells for trVLPs rescue. After the $TCID_{50}$ of trVLPs infectivity was titrated, a serially diluted inhibitor was mixed with trVLPs and incubated at 37 °C for 1 h. After that, the mixture was then inoculated into Caco-2-N cells (MOI = 0.1). Viral infection was measured by flow cytometry (LSRFortessa SORP) at 36 h post infection.

2.10. Synergy analysis of inhibitors

The synergistic effect of P40-LP and IPB24 was determined on Huh-7 cells by the pseudovirus-based single-cycle infection assay as described previously (Ding et al., 2017). Two inhibitors were tested individually or

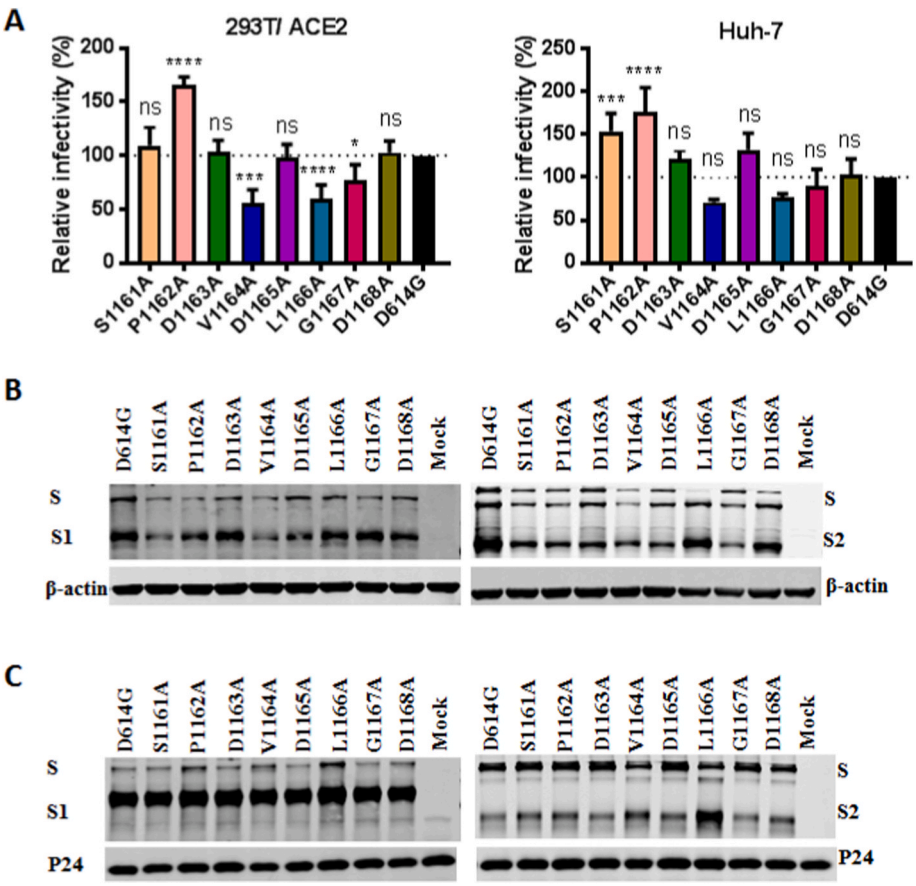

Fig. 3. Infectivity of the S mutants with HR2 mutations. (**A**) Infectivity of SARS-CoV-2 pseudoviruses (PsV) carrying the S mutants in 293T/ACE2 or Huh-7 cells was determined by a single-cycle infection assay. The luciferase activity (RLU) of D614G reference was treated as 100% and the relative infection of an S mutant was accordingly calculated and statistical comparison was conducted one-way ANOVA with Dunnett's multiple comparisons test. The expression profiles of mutant S proteins in transfected 293T cells (**B**) or PsV particles (**C**) were examined by western blotting assays, in which a rabbit anti-S1 (left panel) or anti-S2 (right panel) was used for detection.

in combination at a fixed of 1:1 M ratio based on their IC_{50} values in the inhibition of PsV infection. The cooperative inhibition between them was analyzed using the method of Chou and Talalay (Chou, 2006; Chou and Talalay, 1984). The analysis was performed in a stepwise fashion by calculating IC_{50}s based on the dose-response curves of single inhibitors that were tested separately and two inhibitors tested in combination. The combination index (CI) was calculated with the median-effect equation with the CalcuSyn program to assess the synergistic effect of combinations. CI values were interpreted as follows: A CI of less than 1 indicates synergism (<0.1, very strong synergism; 0.1 to 0.3, strong synergism; 0.3 to 0.7, synergism; 0.7 to 0.85, moderate synergism; and 0.85 to 0.90, slight synergism), a CI of 1 or close to 1 indicates additive effects, and a CI of greater than 1 indicates antagonism.

2.11. Cytotoxicity of inhibitors

The cytotoxicity of P40-LP was measured using Cell-Counting Kit-8 (CCK-8) (Abbkine, Wuhan, China). In brief, cells were seeded on a 96-well tissue culture plate (1×10^4 cells per well), and 50 μl volumes of P40-LP at different concentrations were added to the cells. After incubation at 37 °C for 48 h, 20 μl of CCK-8 solution was added into each well and incubated 2 h at 37 °C. Absorbance at 450 nm was then measured using a Multiskan MK3 microplate reader (Thermo Fisher Scientific, Waltham, MA, USA), and percentage of cell viability was calculated.

2.12. Statistical analysis

The data were analyzed using GraphPad Prism 7 software (GraphPad Software Inc., San Diego, CA, USA). Comparisons of S protein-mediated cell-cell fusion activities and pseudovirus infections were conducted by one-way ANOVA with Dunnett's multiple comparisons test (ns, not significant; *, $p < 0.05$; **, $p < 0.01$; ***, $p < 0.001$; ****, $p < 0.0001$), in which $p < 0.05$ is considered as a significant difference.

3. Results

3.1. The N-terminally extended motif of HR2 is critical for S protein-driven cell fusion

We previously identified that the C-terminal MPER motif of SARS-CoV-2 HR2 plays critical roles in S protein-driven cell fusion and accordingly generated fusion-inhibitory peptides with potent and broad-spectrum activity (Yu et al., 2021a). In this study, we first applied alanine-scanning mutagenesis to characterize the functionality of the HR2 N-terminal motif, the amino acids ^{1161}SPDVDLGD^{1168}. To this end, a plasmid expressing the S protein of D614G reference was used as a template, constructing eight plasmids expressing the S protein with S1161A, P1162A, D1163A, V1164A, D1165A, L1166A, G1167A, or D1168A mutation, respectively. The fusogenic activity of each S mutant was examined by both GFP-based cell fusion assay and DSP-based cell fusion assay. As shown in Fig. 2, all the S mutants exhibited significantly decreased fusogenicity in 293T/ACE2, Huh-7 or Vero E6 cells relative to the D614G reference. Then, we characterized the infectivity of pseudoviruses (PsV) bearing the S mutants by a single-cycle infection assay. In 293T/ACE2 cells, three mutants (V1164A, L1166A, and G1167A) exhibited severely decreased infectivity, whereas P1162A mutant had increased infectivity. In contrast, the infectivity of the S1161A and P1162A mutants in Huh-7 cells increased, whereas others had no significant changes (Fig. 3A). Additionally, we analyzed the protein expression and processing of S mutants in transfected cells or their incorporation in PsV particles by western blotting, using anti-S1 and anti-S2 antibodies. As shown, the S proteins had similar expression profiles in transfected 293T cells (Fig. 3B) and in virions (Fig. 3C), suggesting that the differences of S proteins-driven cell fusion and PsV

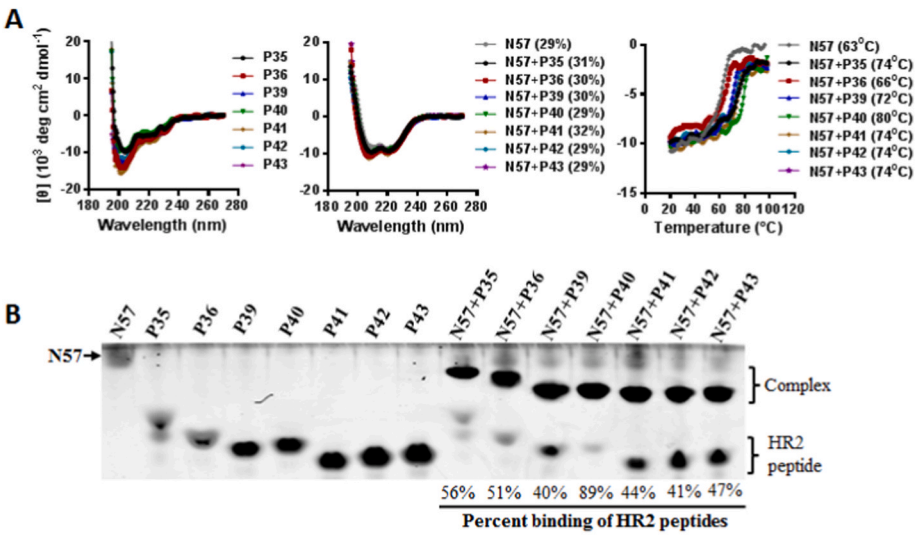

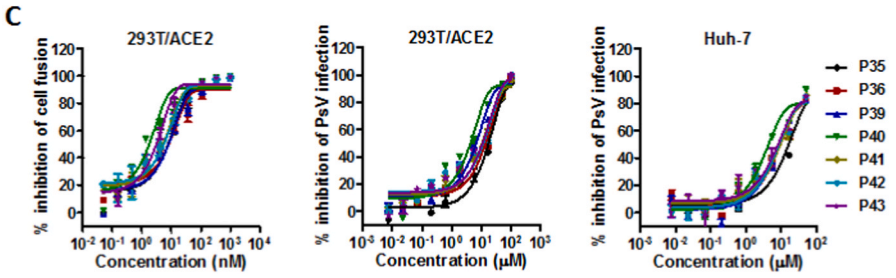

HR2 peptides	IC_{50} ± SD		
	Cell-cell fusion (nM)	PsV on 293T/ACE2 (μM)	PsV on Huh-7 (μM)
P35	8.23 ± 1.51	21.19 ± 0.55	20.24 ± 4.93
P36	**8.44 ± 1.67**	**14.45 ± 2.53**	**8.01 ± 0.97**
P39	8.17 ± 1.21	6.28 ± 1.41	7.93 ± 0.66
P40	**1.46 ± 0.12**	**3.57 ± 0.55**	**3.71 ± 0.97**
P41	5.55 ± 0.86	8.30 ± 0.65	7.32 ± 0.34
P42	**6.43 ± 0.46**	**8.09 ± 0.27**	**6.98 ± 0.59**
P43	3.11 ± 0.14	8.23 ± 1.14	8.64 ± 5.31

Fig. 4. Structural and functional characterization of HR2 peptides with N-terminal extension. (**A**) The α-helicity and thermostability of HR2 peptides alone or in complexes HR1-derived target mimic peptide N57 were determined by Circular dichroism (CD) spectroscopy. (**B**) Visualization of HR2 peptides or their complexes with N57 by N-PAGE analysis. The intensities of peptide bands were analyzed by image J and the binding efficiencies of HR2 with N57 were calculated. (**C**) The inhibitory activities of HR2 peptides against a wild-type (WT) S protein-mediated cell-cell fusion and PsV infection were determined by the DSP-based cell fusion assay and single-cycle infection assay, respectively. For CD spectroscopy and N-PAGE, the experiments were performed two times and obtained consistent results, the representative data are shown. In the inhibition assays, the samples were tested in triplicate and repeated three times, and data are expressed as means ± standard deviations (SD).

infection were not caused by the overexpression system.

3.2. An HR2 peptide with N-terminal extension exhibits obviously enhanced binding activity

To identify potential SARS-CoV-2 fusion inhibitors that possess different pharmaceutical profiles, we synthesized a panel of seven HR2 peptides containing different numbers of N-terminal residues. As illustrated in Fig. 1C, two previously-characterized peptides, P35 and P36, contain the HR2 core sequences only, whereas the new peptides P39, P40, P41, P42, and P43 have an N-terminal extension with three, four, five, six or seven residues. First, we applied CD spectroscopy to characterize the secondary structures of HR2 peptides in the absence or presence of an HR1-derived target mimic peptide N57. As shown in Fig. 4A, HR2 peptides alone exhibited no or minor α-helicity, indicating that they were largely in a random structure. When mixed with an equal molar concentration of N57 peptide, the peptide complexes displayed α-helical contents at ~29–32%. While N57 alone had a helical content of 29% with T_m of 63 °C, the complexes of P35, P41, P42, and P43 peptides showed T_m of 74 °C, the complexes of P36, P39, and P40 showed T_m of 66 °C, 72 °C, and 80 °C, respectively, indicating that P40 peptide had the highest binding stability with N57 peptide.

We also used an N-PAGE method to visualize HR2 peptides and their interactions with N57 peptide. As shown in Fig. 4B, N57 peptide stuck in the well of the gel did not efficiently migrate down because it had a nearly zero net charge, whereas the negatively charged HR2 peptides showed specific bands. When an HR2 peptide and N57 were mixed, new bands corresponding to the binding complexes appeared at the upper positions of the gel, which verified their direct interactions. In comparison, P40 and N57 displayed the highest binding efficiency (89%) among other peptides.

3.3. P40 peptide is the most potent inhibitor of SARS-CoV-2 and emerging variants

We were intrigued to characterize the antiviral activity of various HR2 peptides. For this purpose, both DSP-based cell fusion assay and pseudovirus (PsV)-based single-cycle infection assay were conducted. As shown in Fig. 4C, all the peptides effectively inhibited an ancestral (WT) S protein-driven cell fusions and PsV infections in 293T/ACE2 or Huh-7 cells, with P40 peptide being the most potent inhibitor. Specifically, P40 inhibited the cell fusion with an IC_{50} of 1.46 nM, whereas other peptides had IC_{50} values ranging from 3.11 to 8.44 nM; P40 inhibited PsV infections with an IC_{50} of 3.57 μM in 293T/ACE2 cells and of 3.71 μM in Huh-7 cells, whereas others with IC_{50} values in the range of 6.28–21.19 μM.

Table 1
Inhibitory activities of HR2-derived fusion inhibitors against divergent SARS-CoV-2 variants.

I. HR2 peptides

SARS-CoV-2	Inhibition on cell fusion (IC_{50}, nM)			Inhibition on PsV infection (IC_{50}, μM)		
	P36	P40	P42	P36	P40	P42
D614G	15.66 ± 1.42	2.51 ± 0.09	6.42 ± 0.77	7.88 ± 0.32	1.86 ± 0.31	7.18 ± 0.94
Alpha	10.05 ± 0.28	1.44 ± 0.18	4.59 ± 0.26	6.59 ± 0.35	2.30 ± 0.27	6.78 ± 0.21
Beta	8.23 ± 1.06	1.735 ± 0.11	4.07 ± 0.24	7.05 ± 0.59	2.83 ± 0.16	6.29 ± 0.51
Gamma	9.05 ± 0.78	2.24 ± 0.18	6.69 ± 2.26	6.79 ± 0.78	3.94 ± 0.56	5.57 ± 0.40
Delta	9.27 ± 0.05	2.41 ± 0.37	6.32 ± 0.31	10.84 ± 0.46	2.59 ± 0.48	7.33 ± 0.45
BA.4/5	1.26 ± 0.42	0.40 ± 0.05	0.54 ± 0.02	1.34 ± 0.19	0.41 ± 0.10	1.82 ± 0.20
Mean IC_{50}	8.92	1.79	4.77	6.75	2.32	5.83

II. Lipopeptides

SARS-CoV-2	Inhibition on cell fusion (IC_{50}, nM)			Inhibition on PsV infection (IC_{50}, nM)		
	P40-LP	IPB02V2	IPB24	P40-LP	IPB02V2	IPB24
D614G	0.26 ± 0.02	0.21 ± 0.01	0.20 ± 0.03	3.59 ± 1.21	14.07 ± 0.08	3.21 ± 0.49
BA.1	0.30 ± 0.01	0.32 ± 0.02	0.20 ± 0.01	1.02 ± 0.06	2.45 ± 0.08	1.50 ± 0.34
BA.2	0.43 ± 0.02	0.45 ± 0.06	0.29 ± 0.01	2.00 ± 0.68	3.51 ± 0.30	1.85 ± 0.60
BA.2.12.1	0.42 ± 0.02	0.53 ± 0.04	0.39 ± 0.00	1.48 ± 0.41	3.78 ± 0.07	1.64 ± 0.32
BA.3	0.43 ± 0.01	0.42 ± 0.02	0.33 ± 0.02	2.01 ± 0.63	3.94 ± 0.42	1.71 ± 0.23
BA.4/5	0.43 ± 0.03	0.49 ± 0.01	0.35 ± 0.01	1.84 ± 0.43	3.47 ± 0.52	1.39 ± 0.49
Mean IC_{50}	0.38	0.4	0.29	1.99	5.2	1.88

Samples were tested in triplicate; the experiments were repeated three times, and data are expressed as means ± SD.

Next, we sought to compare the potencies of three representative peptides (P36, P40, and P42) in inhibiting diverse SARS-CoV-2 variants, including the virus bearing a single D614G mutation (D614G reference) and five VOCs (Alpha, Beta, Gamma, Delta, and Omicron BA.4/5). As shown in Table 1 and Fig. S1, P36, P40, and P42 peptides inhibited S protein-driven cell fusions in 293T/ACE2 cells with mean IC_{50} values of 8.92, 1.79, and 4.77 nM, respectively, and inhibited PsV infections in Huh-7 cells with mean IC_{50} values of 6.75, 2.32, and 5.83 μM.

The inhibitory activities of the three peptides were further evaluated in Caco-2 cells, which mediate viral infection mainly through cell surface fusion pathway (Hoffmann et al., 2020b; Koch et al., 2021). As shown in Fig. 5A (upper panel), P36, P40, and P42 inhibited D614G PsV with IC_{50} of 0.27, 0.13, and 0.23 μM, respectively and inhibited BA.4/5 PsV with IC_{50} of 0.15, 0.07, and 0.12 μM, respectively. We also performed an inhibition assay with transcription and replication competent SARS-CoV-2 VLP system (SARS-CoV-2 GFP/ΔN trVLP), which could recapitulate the entire viral life cycle in the Caco-2 cells stably expressing viral nucleocapsid (Caco-2-N) (Ju et al., 2021). In Caco-2-N target cells, P36, P40, and P42 inhibited D614G trVLP with IC_{50} of 0.3, 0.08, and 0.25 μM, respectively and inhibited Omicron BA.1 trVLP with IC_{50} of 0.03, 0.01, and 0.01 μM, respectively (Fig. 5A, lower panel). In comparisons, the peptide inhibitors exerted more efficiently in Caco-2 cells than in 293T/ACE and Huh-7 cells, and P40 displayed the most potent antiviral activity regardless of the cell types.

3.4. Generation and characterization of a highly potent fusion-inhibitory lipopeptide

Previous studies demonstrated that lipid conjugation can dramatically increase the antiviral activity and stability of HR2-derived fusion inhibitory peptides (References). To develop a more efficient inhibitor for clinical use, we designed a novel lipopeptide termed P40-LP by conjugating a cholesterol molecule to the C-terminus of P40 peptide via a flexible PEG_8 linker (Fig. 1C). As shown in Fig. S2, P40-LP displayed an α-helicity of 31% with T_m of 59 °C, and it could interact with N57 peptide to form a more stable complex with the T_m of 87 °C. In the inhibition of cell fusion by the S proteins derived from D614G reference and five Omicron sublineages (Table 1 and Fig. S3), P40-LP had a mean IC_{50} of 0.38 nM, which was comparable to the activities of IPB02V2 (0.4 nM) and IPB24 (0.29 nM). In the inhibition of the corresponding PsV panel, P40-LP, IPB02V2, and IPB24 had IC_{50} of 1.99, 5.2, and 1.88 nM. Moreover, P40-LP also inhibited a group of pseudotyped viruses carrying a single or combined HR1 mutations occurred in Omicron strain very efficiently (Fig. S4).

The inhibitory activities of the lipopeptides were similarly determined with Caco-2 cells. As shown in Fig. 5B, P40-LP, IPB02V2, and IPB24 inhibited D614G PsV with IC_{50} of 0.48, 0.34, and 0.36 nM, respectively and inhibited BA.4/5 PsV with IC_{50} of 0.27, 0.36, and 0.34 nM, respectively. In the inhibition of SARS-CoV-2 trVLP in Caco-2-N cells, P40-LP, IPB02V2, and IPB24 inhibited D614G trVLP with IC_{50} of 4.53, 3.99, and 5.01 nM, respectively, and inhibited Omicron BA.1 trVLP with IC_{50} of 0.31, 0.46, and 0.39 nM, respectively. In comparison, P40-LP exhibited dramatically increased inhibitory activities over the unmodified P40 peptide and the three lipopeptides had similar antiviral activities, confirming the importance of lipopeptide-based strategy for developing membrane fusion inhibitors.

3.5. P40-LP and IPB24 have synergistic effects against SARS-CoV-2 variants

As illustrated in Fig. 1C, while P40-LP was generated with an N-terminal extension, IPB24 was originally designed containing a C-terminal extension. Considering that two lipopeptides target overlapping but different HR1 sites, we were curious whether they possess synergistic effects against SARS-CoV-2 infection. Thus, we determined the inhibitory activities of P40-LP and IPB24 individually or in combination against D614G reference and three Omicron variants by a single-cycle infection assay in Huh-7 cells. As shown in Fig. 6 , the combination of two lipopeptides resulted in synergistic effects in inhibiting D614G (CI = 0.83, moderate synergism), BA.1 (CI = 0.89, slight synergism), BA.2.12.1 (CI = 0.83, moderate synergism), and BA.4/5 (CI = 0.64, synergism). Although no strong synergistic effect (CI < 0.3) was observed between the two inhibitors, the results provide additional implications for the therapeutic strategy of SARS-CoV-2 infection, especially against the currently circulating Omicron variants.

3.6. P40-LP is also a potent inhibitor of other human coronaviruses

We previously demonstrated that IPB02V2 and IPB24 possessed potent, broad-spectrum inhibitory activities against other human coronaviruses, including SARS-CoV, MERS-CoV, HCoV-229E, and HCoV-NL63 (Yu et al., 2021a; Zhu et al., 2021). In order to characterize the breadth and potency of P40-LP, the pseudotypes of SARS-CoV, MERS-CoV, HCoV-229E, and HCoV-NL63 were prepared and single-cycle infection assay was similarly conducted in Huh-7 cells. As shown in Fig. 7, P40-LP, IPB02V2 and IPB24 inhibited SARS-CoV with IC_{50} of 10.23, 48.16, and 9.21 nM, respectively; inhibited MERS-CoV with IC_{50} of 41.68, 56.17, and 35.82 nM, respectively; inhibited HCoV-229E with IC_{50} of 389.14, 676.26, and 603.77 nM, respectively; and inhibited HCoV-NL63 with IC_{50} of 36.05, 100.32, and 574.72 nM, respectively. Therefore, P40-LP was more potent than IPB02V2 against the infection

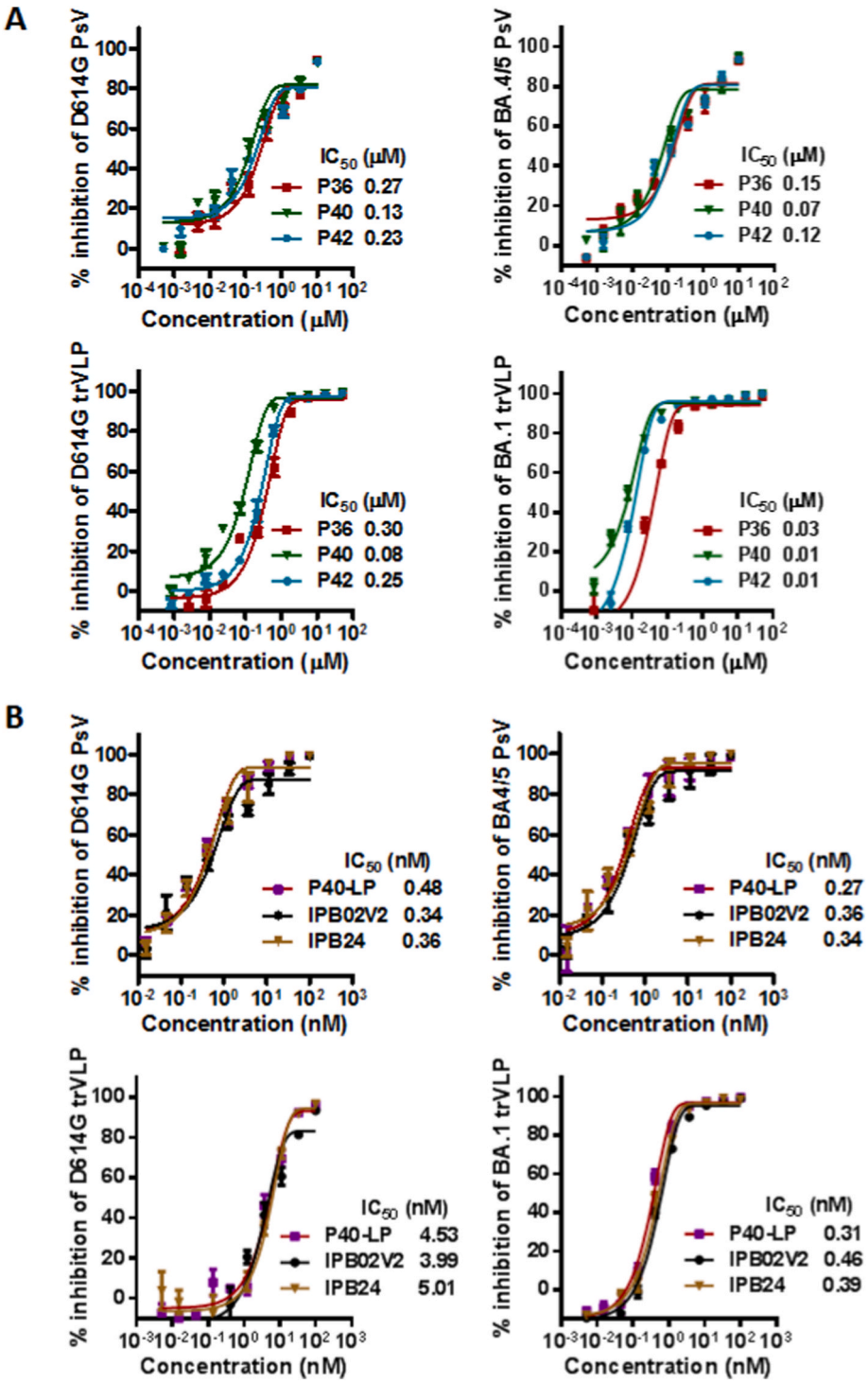

Fig. 5. Inhibitory activities of HR2-based fusion inhibitors in Caco-2 cells. The inhibitory activities of representative fusion-inhibitory peptides (**A**) and lipopeptides (**B**) against the infections of D614G or BA.4/5 PsV (upper panel) and live D614G or BA.1 trVLP (lower panel) were respectively measured. The experiments were repeated three times, and data are expressed as means ± SD.

of the four human CoVs, implying the critical roles of the N-terminally extended HR2 sequences in the antiviral activity. Additionally, P40-LP showed more potent inhibition than IPB24 on HCoV-229E and HCoV-NL63 infections.

3.7. Cytotoxicity and stability of P40-LP

In order to validate the antiviral potency of P40-LP, we measured its cytotoxicity in the target cells that were used in the above inhibition assays. As shown in Fig. S5A, P40-LP at a concentration of 1 μM or 5 μM exhibited no appreciable cytotoxicity in 293T/ACE2, Huh-7, and Caco-2 cells, but it resulted in greatly reduced cell viability when its concentration was raised to 10 μM. This result suggested that P40-LP has relatively low cytotoxicity and high therapeutic selection index (CC_{50}/IC_{50}).

Furthermore, the *in vitro* stability of P40-LP was characterized, in which the lipopeptide was treated with different experimental conditions and its antiviral activity was then determined by D614G PsV-based

A

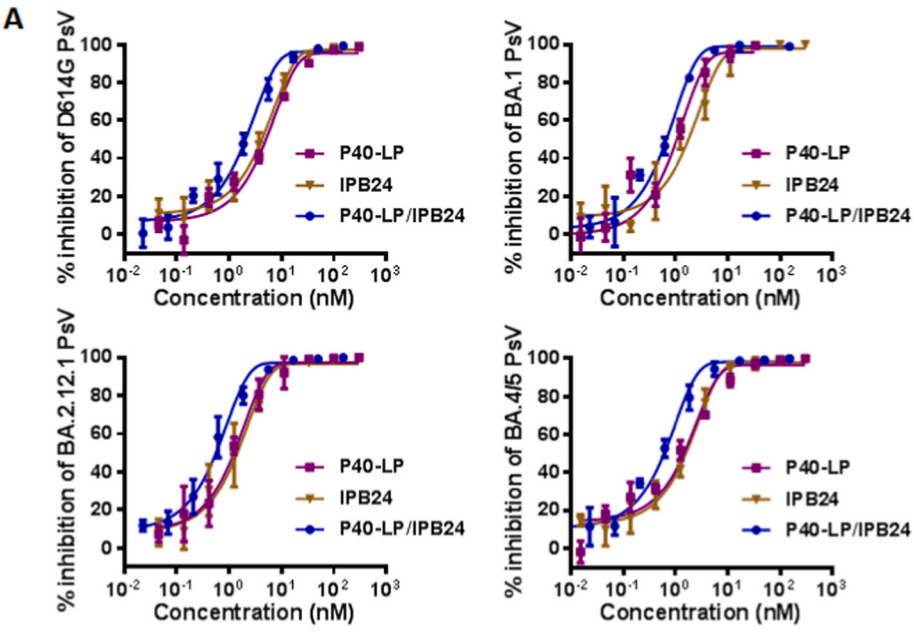

B

PsV	IC_{50} ± SD			
	P40-LP	IPB24	P40-LP/IPB24	CI
D614G	4.78 ± 0.49	4.35 ± 0.79	1.88 ± 0.05	**0.83**
BA.1	1.14 ± 0.18	1.65 ± 0.20	0.60 ± 0.05	**0.89**
BA.2.12.1	1.26 ± 0.23	1.35 ± 0.32	0.54 ± 0.08	**0.83**
BA.4/5	1.36 ± 0.10	2.13 ± 0.22	0.53 ± 0.14	**0.64**

Fig. 6. Synergistic effects between P40-LP and IPB24 lipopeptides. (**A**) The inhibition curves of P40-LP and IPB24 individually or in combination against the infections of D614G reference and three Omicron variants were determined by PsV-based single-cycle infection assay. (**B**) The IC_{50} values from three independent experiments are presented as means ± SD.

single-cycle infection assay. For its thermostability, P40-LP solution was stored at 4 °C, room temperature (RT) or 37 °C for two weeks; the results demonstrated that its inhibitory activity was almost unchanged (Fig. S5B). To assess its sensitivity to proteolytic enzymes, P40-LP (2 mg/ml) was treated with proteinase K, trypsin or chymotrypsin at 37 °C over 4 h; the results suggested that the lipopeptide could largely tolerate the digestion of chymotrypsin, but not proteinase K and trypsin (Fig. S5C). When P40-LP was incubated with 20% human serum at 37 °C, its inhibitory activity was largely maintained either (Fig. S5D).

4. Discussion

In this study, we comprehensively characterized the functionality of the N-terminally extended motif of HR2 in SARS-CoV-2. First, the N-terminally extended motif was identified to be critical for S protein-mediated cell fusion. A group of new HR2 peptides containing different numbers of N-terminally extended residues were synthesized and characterized for their antiviral activities. As shown, P40 peptide was found to be the most robust inhibitor in terms of both binding and inhibitory activities. Subsequently, a lipopeptide termed P40-LP was designed by conjugating P40 with cholesterol, which exhibited dramatically increased activities in inhibiting divergent SARS-CoV-2 variants. Moreover, P40-LP had a certain degree of synergistic effect with the C-terminally extended lipopeptide IPB24, and it also effectively inhibited other human coronaviruses, including SARS-CoV, MERS-CoV, HCoV-229E, and HCoV-NL63. In conclusion, our studies have not only established the roles of the N-terminally extended HR2 motif in SARS-CoV-2 fusion and its inhibition, but also provided novel antivirals that can be further developed for clinical use.

The residues 1168–1203 of SARS-CoV-2 HR2 are considered as the core sequence to form the six-helical bundle structure required for viral fusion and infection; thus, the peptide P35 or P36 has been primarily used as a template to develop fusion inhibitors, such as IPB01 (Zhu et al., 2020), P3 (Sun et al., 2020), 2019-nCoV-HR2P (Xia et al., 2020b), and SARS-CoV-2-HRC (Outlaw et al., 2020). Consistently, these P35- and P36-based unmodified peptides exhibited a very low antiviral activity, with the IC_{50} values at macromolar (μM) levels. To our surprise, Yang et al. recently reported an N-terminally extended, unmodified HR2 peptide, termed longHR2_42 (namely P42 in this work), which could inhibit SARS-CoV-2 and its variants with IC_{50} at single-digit nanomolar (nM) levels in cell-based and virus-based assays (Yang et al., 2022a). Moreover, their studies showed that longHR2_42 was ~100-fold more potent than shortHR2 (namely P36 peptide here), thus claiming it as the most potent peptide inhibitor to date (Yang et al., 2022a). Contradictorily, our studies showed that P42 and P36 peptides had similar inhibitory activities; rather, P40 peptide, which was truncated two N-terminal residues from P42, exhibited improved potencies in inhibiting SARS-CoV-2 and several variants of concern (VOCs), as determined by different experimental systems. Actually, we previously achieved the preliminary results on the characterization of the N-terminally extended HR2 motif, which revealed the inability of the peptide P41 to improve the antiviral activity, thus we later dedicated to develop more effective inhibitors containing the C-terminal extension (Yu et al., 2021a). To address the differences, we afterwards synthesized the panel of peptides including P39, P40, P42, and P43; among them, only P40 was identified with improved binding and inhibitory activities relative to the previously published P36 or P35 peptide (Outlaw et al., 2020; Sun et al., 2020; Xia et al., 2020b; Zhu et al., 2020). Definitely, our data presented

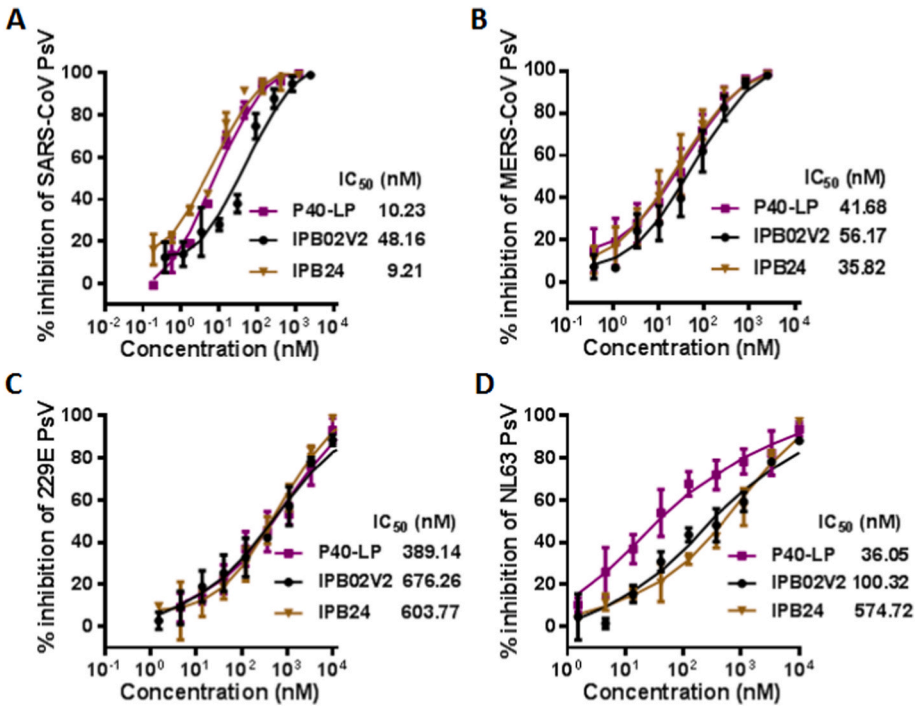

Fig. 7. Inhibitory activities of lipopeptides against other human coronaviruses. The inhibitory activities of P40-LP along with IPB02V2 and IPB24 against SARS-CoV (**A**), MERS-CoV (**B**), HCoV-229E (**C**) and HCoV-NL63 (**D**) were determined in Huh-7 cells by PsV-based single-cycle infection assays. The experiments were repeated three times, and data are expressed as means ± SD.

here have provided crucial information for understanding the structure-activity relationship (SAR) of SARS-CoV-2 HR2; the reasons that led to the disparity with the longHR2_42 and shortHR2 need to be cautiously investigated in the future.

SARS-CoV-2 infects cells through either directly fusing with plasma membrane (cell surface pathway) or undergoing endocytosis traveling to endosome for membrane fusion (endosome pathway), which is mediated by the trimeric S protein: while S1 subunit is responsible for receptor binding, its S2 subunit mediates membrane fusion by forming a 6-HB conformation that juxtaposes the viral and cell membranes for merging (Walls et al., 2020; Wrapp et al., 2020). In the cells with high TMPRSS2 expression, SARS-CoV-2 predominantly uses the TMPRSS2-mediated plasma membrane entry pathway, but the virus can alternatively enter through endosome pathway mediated by endosomal proteases such as cathepsin L in the cells with low or no TMPRSS2 expression (Beumer et al., 2021; Hoffmann et al., 2020a, 2020b; Koch et al., 2021). Previous studies have demonstrated that while an unmodified native HR2 peptide can block cell surface pathway, instead of endosomal pathway, lipid conjugation also enables activity against viruses that do not fuse until they have been taken up via endocytosis (Lee et al., 2011; Ujike et al., 2008). A lipopeptide can bind to both the viral and cell membranes, which greatly elevates the local concentration of the inhibitor thus enhancing the antiviral activity dramatically (Chong et al., 2018b; Zhu et al., 2019, 2023). Also, such the case sharply increases the stability of peptide drug that confers a significantly extended *in vivo* half-life (Chong et al., 2017, 2018a, 2019; Xue et al., 2022). In this study, we found that in the inhibition of various SARS-CoV-2 PsV infections, the cholesterol-modified lipopeptide P40-LP was ~1166-fold more potent than P40 in Huh-7 cells (Table 1) and ~271- or ~259-fold more potent than P40 in Caco-2 cells (Fig. 5). Consistently, P40-LP was ~32- or 18-fold more potent than P40 in inhibiting SARS-CoV-2 GFP/ΔN trVLP in Caco-2-N cells (Fig. 5). It is largely dependent on TMPRSS2, Huh-7 cells can mediate both the cell surface and endosomal entry pathways, whereas Caco-2 cells are mainly infected through the cell surface pathway (Chu et al., 2021; Hoffmann et al., 2020b; Hu et al., 2022); thus, it is conceivable that both P40 and P40-LP inhibitors were more active in Caco-2 cells than in Huh-7 cells, and that P40-LP exhibited additional advantages in Huh-7 cells through the binding of viral and cell membranes to enter target cells. This concept is also justified by the inhibitory results of cell-cell fusion driven by S protein, in which P40-LP only exhibited ~5-fold increased potency over P40 (Table 1).

Given that SARS-CoV-2 mutates easily resulting in many variants of concern, especially Omicron sublineages, the fusion-inhibitory peptides or lipopeptides were further verified to possess the broad-spectrum antiviral activity with high potency. Furthermore, our studies also found that P40-LP and the previously developed lipopeptide IPB24 possessed comparable inhibitory activities against divergent SARS-CoV-2 variants, and importantly, they displayed different levels of synergy, thus offering an optional strategy for combination therapy. Moreover, the inhibitory activities of P40-LP on SARS-CoV-2, MERS-CoV-2, HCoV-229E, and HCoV-NL63 further support the concept developing a pan-coronavirus inhibitor, which should be in preparedness to battle against the emergence or re-emergence of new viruses from animal reservoirs. Last, we would like emphasize that we will continue our efforts to investigate P40-based inhibitors in details, including both the *in vitro* and *in vivo* antiviral activities and potential side-effects. Considering that P40-LP cannot tolerate the *in vitro* digestions of proteinase K and trypsin, it is important to determine its pharmacokinetics in animals; thus, an optimization strategy might be undertaken to improve the sequence or structure stability of P40-LP and solidify its druggability for clinical development.

Author contributions

Y.H., Y.Z., Y.Y., N.L., and X.J. performed the experiments. Y. H., Y.Z., Q.D. and Y.He analyzed the data. Q.D. and Y.He supervised the study. Y. He. designed the study and wrote the manuscript with Y.H. and Q.D.. All authors read and approved the submitted version.

Declaration of competing interest

The authors declare that they have no known competing financial interests or personal relationships that could have appeared to influence the work reported in this paper.

Data availability

Data will be made available on request.

Acknowledgements

We thank Linqi Zhang at the Tsinghua University (Beijing, China) for providing the plasmids that encode the S proteins of various SARS-CoV-2 VOCs, and Zene Matsuda at the Institute of Medical Science, University of Tokyo (Tokyo, Japan) for providing the DSP1-7 and DSP8-11 plasmids used in the cell-cell fusion assay. This work was supported by grants from the CAMS Innovation Fund for Medical Sciences (2022-I2M-1–021) and the National Natural Science Foundation of China (82221004, 82230076).

Appendix A. Supplementary data

Supplementary data to this article can be found online at https://doi.org/10.1016/j.antiviral.2023.105571.

References

Beumer, J., Geurts, M.H., Lamers, M.M., Puschhof, J., Zhang, J., van der Vaart, J., Mykytyn, A.Z., Breugem, T.I., Riesebosch, S., Schipper, D., van den Doel, P.B., de Lau, W., Pleguezuelos-Manzano, C., Busslinger, G., Haagmans, B.L., Clevers, H., 2021. A CRISPR/Cas9 genetically engineered organoid biobank reveals essential host factors for coronaviruses. Nat. Commun. 12, 5498.

Cao, Y., Yisimayi, A., Jian, F., Song, W., Xiao, T., Wang, L., Du, S., Wang, J., Li, Q., Chen, X., Yu, Y., Wang, P., Zhang, Z., Liu, P., An, R., Hao, X., Wang, Y., Wang, J., Feng, R., Sun, H., Zhao, L., Zhang, W., Zhao, D., Zheng, J., Yu, L., Li, C., Zhang, N., Wang, R., Niu, X., Yang, S., Song, X., Chai, Y., Hu, Y., Shi, Y., Zheng, L., Li, Z., Gu, Q., Shao, F., Huang, W., Jin, R., Shen, Z., Wang, Y., Wang, X., Xiao, J., Xie, X.S., 2022. BA.2.12.1, BA.4 and BA.5 escape antibodies elicited by Omicron infection. Nature 608, 593–602.

Chong, H., Xue, J., Xiong, S., Cong, Z., Ding, X., Zhu, Y., Liu, Z., Chen, T., Feng, Y., He, L., Guo, Y., Wei, Q., Zhou, Y., Qin, C., He, Y., 2017. A lipopeptide HIV-1/2 fusion inhibitor with highly potent in vitro, ex vivo, and in vivo antiviral activity. J. Virol. 91, e00288-00217.

Chong, H., Xue, J., Zhu, Y., Cong, Z., Chen, T., Guo, Y., Wei, Q., Zhou, Y., Qin, C., He, Y., 2018a. Design of novel HIV-1/2 fusion inhibitors with high therapeutic efficacy in rhesus monkey models. J. Virol. 92, e00775-00718.

Chong, H., Xue, J., Zhu, Y., Cong, Z., Chen, T., Wei, Q., Qin, C., He, Y., 2019. Monotherapy with a low-dose lipopeptide HIV fusion inhibitor maintains long-term viral suppression in rhesus macaques. PLoS Pathog. 15, e1007552.

Chong, H., Zhu, Y., Yu, D., He, Y., 2018b. Structural and functional characterization of membrane fusion inhibitors with extremely potent activity against HIV-1, HIV-2, and simian immunodeficiency virus. J. Virol. 92, e01088-01018.

Chou, T.C., 2006. Theoretical basis, experimental design, and computerized simulation of synergism and antagonism in drug combination studies. Pharmacol. Rev. 58, 621–681.

Chou, T.C., Talalay, P., 1984. Quantitative analysis of dose-effect relationships: the combined effects of multiple drugs or enzyme inhibitors. Adv. Enzym. Regul. 22, 27–55.

Chu, H., Hu, B., Huang, X., Chai, Y., Zhou, D., Wang, Y., Shuai, H., Yang, D., Hou, Y., Zhang, X., Yuen, T.T., Cai, J.P., Zhang, A.J., Zhou, J., Yuan, S., To, K.K., Chan, I.H., Sit, K.Y., Foo, D.C., Wong, I.Y., Ng, A.T., Cheung, T.T., Law, S.Y., Au, W.K., Brindley, M.A., Chen, Z., Kok, K.H., Chan, J.F., Yuen, K.Y., 2021. Host and viral determinants for efficient SARS-CoV-2 infection of the human lung. Nat. Commun. 12, 134.

Ding, X., Zhang, X., Chong, H., Zhu, Y., Wei, H., Wu, X., He, J., Wang, X., He, Y., 2017. Enfuvirtide (T20)-based lipopeptide is a potent HIV-1 cell fusion inhibitor: implication for viral entry and inhibition. J. Virol. 91, e00831-00817.

Fan, Y., Li, X., Zhang, L., Wan, S., Zhang, L., Zhou, F., 2022. SARS-CoV-2 Omicron variant: recent progress and future perspectives. Signal Transduct. Targeted Ther. 7, 141.

Guo, Y., Han, J., Zhang, Y., He, J., Yu, W., Zhang, X., Wu, J., Zhang, S., Kong, Y., Guo, Y., Lin, Y., Zhang, J., 2022. SARS-CoV-2 omicron variant: epidemiological features, biological characteristics, and clinical significance. Front. Immunol. 13, 877101.

He, Y., Cheng, J., Lu, H., Li, J., Hu, J., Qi, Z., Liu, Z., Jiang, S., Dai, Q., 2008a. Potent HIV fusion inhibitors against Enfuvirtide-resistant HIV-1 strains. Proc. Natl. Acad. Sci. U.S.A. 105, 16332–16337.

He, Y., Xiao, Y., Song, H., Liang, Q., Ju, D., Chen, X., Lu, H., Jing, W., Jiang, S., Zhang, L., 2008b. Design and evaluation of sifuvirtide, a novel HIV-1 fusion inhibitor. J. Biol. Chem. 283, 11126–11134.

Hoffmann, M., Kleine-Weber, H., Pohlmann, S., 2020a. A multibasic cleavage site in the spike protein of SARS-CoV-2 is essential for infection of human lung cells. Mol. Cell 78, 779–784 e775.

Hoffmann, M., Kleine-Weber, H., Schroeder, S., Kruger, N., Herrler, T., Erichsen, S., Schiergens, T.S., Herrler, G., Wu, N.H., Nitsche, A., Muller, M.A., Drosten, C., Pohlmann, S., 2020b. SARS-CoV-2 cell entry depends on ACE2 and TMPRSS2 and is blocked by a clinically proven protease inhibitor. Cell 181, 271–280 e278.

Hu, B., Chan, J.F., Liu, H., Liu, Y., Chai, Y., Shi, J., Shuai, H., Hou, Y., Huang, X., Yuen, T. T., Yoon, C., Zhu, T., Zhang, J., Li, W., Zhang, A.J., Zhou, J., Yuan, S., Zhang, B.Z., Yuen, K.Y., Chu, H., 2022. Spike mutations contributing to the altered entry preference of SARS-CoV-2 omicron BA.1 and BA.2. Emerg. Microb. Infect. 11, 2275–2287.

Ju, X., Zhu, Y., Wang, Y., Li, J., Zhang, J., Gong, M., Ren, W., Li, S., Zhong, J., Zhang, L., Zhang, Q.C., Zhang, R., Ding, Q., 2021. A novel cell culture system modeling the SARS-CoV-2 life cycle. PLoS Pathog. 17, e1009439.

Koch, J., Uckeley, Z.M., Doldan, P., Stanifer, M., Boulant, S., Lozach, P.Y., 2021. TMPRSS2 expression dictates the entry route used by SARS-CoV-2 to infect host cells. EMBO J. 40, e107821.

Lalezari, J.P., Henry, K., O'Hearn, M., Montaner, J.S., Piliero, P.J., Trottier, B., Walmsley, S., Cohen, C., Kuritzkes, D.R., Eron Jr., J.J., Chung, J., DeMasi, R., Donatacci, L., Drobnes, C., Delehanty, J., Salgo, M., Group, T.S., 2003. Enfuvirtide, an HIV-1 fusion inhibitor, for drug-resistant HIV infection in North and South America. N. Engl. J. Med. 348, 2175–2185.

Lee, K.K., Pessi, A., Gui, L., Santoprete, A., Talekar, A., Moscona, A., Porotto, M., 2011. Capturing a fusion intermediate of influenza hemagglutinin with a cholesterol-conjugated peptide, a new antiviral strategy for influenza virus. J. Biol. Chem. 286, 42141–42149.

Markov, P.V., Katzourakis, A., Stilianakis, N.I., 2022. Antigenic evolution will lead to new SARS-CoV-2 variants with unpredictable severity. Nat. Rev. Microbiol. 20, 251–252.

Outlaw, V.K., Bovier, F.T., Mears, M.C., Cajimat, M.N., Zhu, Y., Lin, M.J., Addetia, A., Lieberman, N.A.P., Peddu, V., Xie, X., Shi, P.Y., Greninger, A.L., Gellman, S.H., Bente, D.A., Moscona, A., Porotto, M., 2020. Inhibition of coronavirus entry in vitro and ex vivo by a lipid-conjugated peptide derived from the SARS-CoV-2 spike glycoprotein HRC domain. mBio 11, e01935-01920.

Qu, P., Faraone, J., Evans, J.P., Zou, X., Zheng, Y.M., Carlin, C., Bednash, J.S., Lozanski, G., Mallampalli, R.K., Saif, L.J., Oltz, E.M., Mohler, P.J., Gumina, R.J., Liu, S.L., 2022. Neutralization of the SARS-CoV-2 omicron BA.4/5 and BA.2.12.1 subvariants. N. Engl. J. Med. 386, 2526–2528.

Shrestha, L.B., Foster, C., Rawlinson, W., Tedla, N., Bull, R.A., 2022. Evolution of the SARS-CoV-2 omicron variants BA.1 to BA.5: implications for immune escape and transmission. Rev. Med. Virol. 32, e2381.

Sun, H., Li, Y., Liu, P., Qiao, C., Wang, X., Wu, L., Liu, K., Hu, Y., Su, C., Tan, S., Zou, S., Wu, G., Yan, J., Gao, G.F., Qi, J., Wang, Q., 2020. Structural basis of HCoV-19 fusion core and an effective inhibition peptide against virus entry. Emerg. Microb. Infect. 9, 1238–1241.

Tang, T., Bidon, M., Jaimes, J.A., Whittaker, G.R., Daniel, S., 2020. Coronavirus membrane fusion mechanism offers a potential target for antiviral development. Antivir. Res. 178, 104792.

Ujike, M., Nishikawa, H., Otaka, A., Yamamoto, N., Yamamoto, N., Matsuoka, M., Kodama, E., Fujii, N., Taguchi, F., 2008. Heptad repeat-derived peptides block protease-mediated direct entry from the cell surface of severe acute respiratory syndrome coronavirus but not entry via the endosomal pathway. J. Virol. 82, 588–592.

Uraki, R., Kiso, M., Iida, S., Imai, M., Takashita, E., Kuroda, M., Halfmann, P.J., Loeber, S., Maemura, T., Yamayoshi, S., Fujisaki, S., Wang, Z., Ito, M., Ujie, M., Iwatsuki-Horimoto, K., Furusawa, Y., Wright, R., Chong, Z., Ozono, S., Yasuhara, A., Ueki, H., Sakai-Tagawa, Y., Li, R., Liu, Y., Larson, D., Koga, M., Tsutsumi, T., Adachi, E., Saito, M., Yamamoto, S., Hagihara, M., Mitamura, K., Sato, T., Hojo, M., Hattori, S.I., Maeda, K., Valdez, R., team, I.s., Okuda, M., Murakami, J., Duong, C., Godbole, S., Douek, D.C., Maeda, K., Watanabe, S., Gordon, A., Ohmagari, N., Yotsuyanagi, H., Diamond, M.S., Hasegawa, H., Mitsuya, H., Suzuki, T., Kawaoka, Y., 2022. Characterization and antiviral susceptibility of SARS-CoV-2 Omicron BA.2. Nature 607, 119–127.

Walls, A.C., Park, Y.J., Tortorici, M.A., Wall, A., McGuire, A.T., Veesler, D., 2020. Structure, function, and antigenicity of the SARS-CoV-2 spike glycoprotein. Cell 181, 281–292 e286.

Wang, P., Nair, M.S., Liu, L., Iketani, S., Luo, Y., Guo, Y., Wang, M., Yu, J., Zhang, B., Kwong, P.D., Graham, B.S., Mascola, J.R., Chang, J.Y., Yin, M.T., Sobieszczyk, M., Kyratsous, C.A., Shapiro, L., Sheng, Z., Huang, Y., Ho, D.D., 2021. Antibody resistance of SARS-CoV-2 variants B.1.351 and B.1.1.7. Nature 593, 130–135.

Wild, C.T., Shugars, D.C., Greenwell, T.K., McDanal, C.B., Matthews, T.J., 1994. Peptides corresponding to a predictive alpha-helical domain of human immunodeficiency virus type 1 gp41 are potent inhibitors of virus infection. Proc. Natl. Acad. Sci. U.S.A. 91, 9770–9774.

Wrapp, D., Wang, N., Corbett, K.S., Goldsmith, J.A., Hsieh, C.L., Abiona, O., Graham, B. S., McLellan, J.S., 2020. Cryo-EM structure of the 2019-nCoV spike in the prefusion conformation. Science 367, 1260–1263.

Xia, S., Liu, M., Wang, C., Xu, W., Lan, Q., Feng, S., Qi, F., Bao, L., Du, L., Liu, S., Qin, C., Sun, F., Shi, Z., Zhu, Y., Jiang, S., Lu, L., 2020a. Inhibition of SARS-CoV-2 (previously 2019-nCoV) infection by a highly potent pan-coronavirus fusion inhibitor targeting its spike protein that harbors a high capacity to mediate membrane fusion. Cell Res. 30, 343–355.

Xia, S., Zhu, Y., Liu, M., Lan, Q., Xu, W., Wu, Y., Ying, T., Liu, S., Shi, Z., Jiang, S., Lu, L., 2020b. Fusion mechanism of 2019-nCoV and fusion inhibitors targeting HR1 domain in spike protein. Cell. Mol. Immunol. 17, 765–767.

Xue, J., Chong, H., Zhu, Y., Zhang, J., Tong, L., Lu, J., Chen, T., Cong, Z., Wei, Q., He, Y., 2022. Efficient treatment and pre-exposure prophylaxis in rhesus macaques by an HIV fusion-inhibitory lipopeptide. Cell 185, 131–144 e118.

Yang, K., Wang, C., Kreutzberger, A.J.B., Ojha, R., Kuivanen, S., Couoh-Cardel, S., Muratcioglu, S., Eisen, T.J., White, K.I., Held, R.G., Subramanian, S., Marcus, K., Pfuetzner, R.A., Esquivies, L., Doyle, C.A., Kuriyan, J., Vapalahti, O., Balistreri, G., Kirchhausen, T., Brunger, A.T., 2022a. Nanomolar inhibition of SARS-CoV-2 infection by an unmodified peptide targeting the prehairpin intermediate of the spike protein. Proc. Natl. Acad. Sci. U.S.A. 119, e2210990119.

Yang, K., Wang, C., White, K.I., Pfuetzner, R.A., Esquivies, L., Brunger, A.T., 2022b. Structural conservation among variants of the SARS-CoV-2 spike postfusion bundle. Proc. Natl. Acad. Sci. U.S.A. 119, e2119467119.

Yu, D., Zhu, Y., Jiao, T., Wu, T., Xiao, X., Qin, B., Chong, H., Lei, X., Ren, L., Cui, S., Wang, J., He, Y., 2021a. Structure-based design and characterization of novel fusion-inhibitory lipopeptides against SARS-CoV-2 and emerging variants. Emerg. Microb. Infect. 10, 1227–1240.

Yu, D., Zhu, Y., Yan, H., Wu, T., Chong, H., He, Y., 2021b. Pan-coronavirus fusion inhibitors possess potent inhibitory activity against HIV-1, HIV-2, and simian immunodeficiency virus. Emerg. Microb. Infect. 10, 810–821.

Zhu, Y., Chong, H., Yu, D., Guo, Y., Zhou, Y., He, Y., 2019. Design and characterization of cholesterylated peptide HIV-1/2 fusion inhibitors with extremely potent and long-lasting antiviral activity. J. Virol. 93, e02312-02318.

Zhu, Y., Dong, X., Liu, N., Wu, T., Chong, H., Lei, X., Ren, L., Wang, J., He, Y., 2022a. SARS-CoV-2 fusion-inhibitory lipopeptides maintain high potency against divergent variants of concern including Omicron. Emerg. Microb. Infect. 11, 1819–1827.

Zhu, Y., Hu, Y., Liu, N., Chong, H., He, Y., 2022b. Potent inhibition of diverse Omicron sublineages by SARS-CoV-2 fusion-inhibitory lipopeptides. Antivir. Res. 208, 105445.

Zhu, Y., Li, M., Liu, N., Wu, T., Han, X., Zhao, G., He, Y., 2023. Development of highly effective LCB1-based lipopeptides targeting the spike receptor-binding motif of SARS-CoV-2. Antivir. Res. 211, 105541.

Zhu, Y., Yu, D., Hu, Y., Wu, T., Chong, H., He, Y., 2021. SARS-CoV-2-derived fusion inhibitor lipopeptides exhibit highly potent and broad-spectrum activity against divergent human coronaviruses. Signal Transduct. Targeted Ther. 6, 294.

Zhu, Y., Yu, D., Yan, H., Chong, H., He, Y., 2020. Design of potent membrane fusion inhibitors against SARS-CoV-2, an emerging coronavirus with high fusogenic activity. J. Virol. 94, e00635-00620.